DEVELOPMENT OF AN IN-VIVO ACOUSTIC DIAGNOSTIC FOR LITHOTRIPTER-INDUCED SHOCK-TISSUE INTERACTION (GR/N19243/01**)**

1. BACKGROUND

Extracorporeal shock wave lithotripsy (ESWL) is the preferred treatment for most kidney stones [1]. Several thousand shocks are focused onto the stone and, mainly through cavitation, break it down into fragments small enough to be passed naturally from the body (during urination), or dissolved with drugs [2]. Currently the shock wave focus is aligned with the stone at the start of the procedure using X-rays or ultrasound (although the images are not simple to interpret – Fig.1). Although the alignment might degrade during treatment as a result of patient or stone motion, subsequent checks of targeting accuracy are rarely possible because of X-ray exposure limitations. The first goal of this contract was to devise a passive instrument which could continually monitor this targeting. In addition, current practice exposes each stone to a fixed number of shocks (generated at a rate of 1-2 s^{-1}), with no feedback available as to the degree of stone fragmentation. Hence the second goal of the passive device was to provide such feedback continuously. This would improve the procedure in a number of ways. If too few shocks are given to fragment the stone, the patient requires re-treatment, with commensurate costs in terms of finance, patient discomfort and waiting times, waiting lists, theatre time and resources (both facilities and staff). Currently >50% of patients require re-treatment. If the fixed number of shocks is greater than that required to fragment the stone sufficiently, this also wastes theatre and staff time. Furthermore, healthy tissue is unnecessarily exposed to the destructive shock waves, and the lithotripter shock wave source (which has a lifetime of a set number of shocks, and currently is replaced at a cost of thousands of pounds every few months) suffers unnecessary wear-and-tear [3].

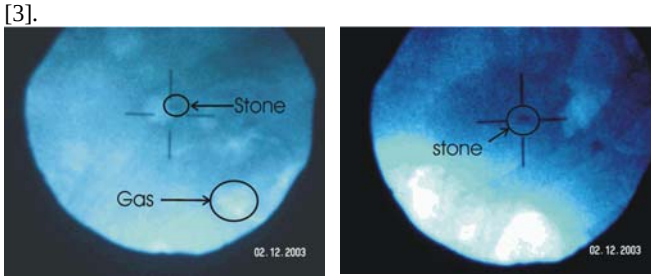

Fig. 1*. X-ray image of a stone (and gas) before (left) and after (right) lithotripsy treatment.*

Two schemes were devised to interpret the output of the device. First, an empirical scheme provided the surgeon with audio information from a loudspeaker in the theatre, so that he/she could 'learn' what sounds were characteristic of a successful treatment. Second, computation fluid dynamics (CFD) simulations were performed to improve understanding of how the signal detected by the device related to the conditions within the patient. The latter route would clearly have great potential for advancing other areas of science (and indeed has lead to further grants in sonochemistry and erosion studies).

2. KEY ADVANCES AND SUPPORTING METHODOLOGY

2.1 Key advances: Summary

In 1992-4, two of the investigators (Coleman and Leighton) correlated luminescent and acoustic emissions from the focus of a lithotripter to show that, under the influence of a lithotripter shock wave, a given bubble will emit two main shock waves, separated by about 200-300 μs [4,5]. Each shock wave signifies the end-point of a bubble collapse, the first being induced (at ~t=0 in Fig. 2) by the compressive shock wave from the lithotripter [6]. The bubble then rebounds, expands, and then collapses again, emitting a second shock wave (at ~t=220 μs in Fig. 2). When a multitude of bubbles follow this pattern, with a range of timings as result of their different locations and sizes, the characteristic 'double-burst' signal is detected (Fig. 3). One source of these shock waves is as follows. Cavitation bubbles close to the kidney stone involute on collapse, forming a jet. This jet may impact the stone directly or, if the bubble is further from the stone, will impact the far bubble wall, and a blast wave will be emitted. The device produced by this project operated by detecting the acoustic pressure signals generated by the cavitation. These differ depending on the accuracy of the targeting, and the degree of fragmentation of the stone.

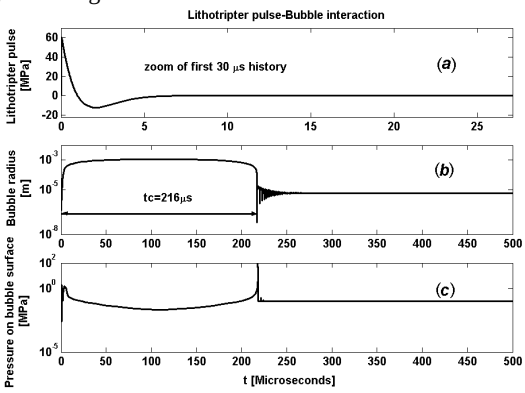

Fig. 2. *The top graph shows an idealised lithotripter pulse. On a longer common time axis the bubble radius (middle row) and the predicted pressure in the liquid at the bubble wall (bottom row) are shown, as calculated by the Gilmore-Akulichev model for a single bubble of initial radius 6 microns.*

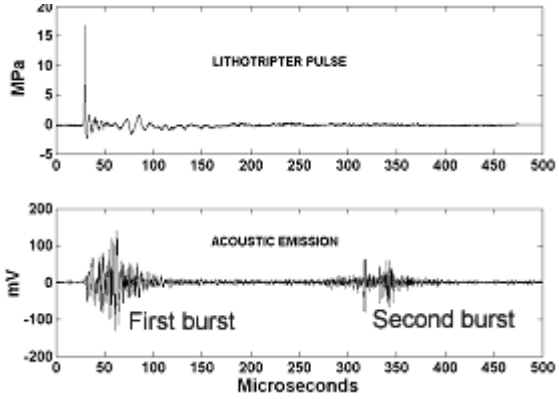

Fig. 3. *A measured lithotripter pulse (upper plot) and a simultaneous output from a cavitation detector in vitro (lower plot). After the 'first burst' of cavitation emissions (which can be compared in form to the later simulated 'first burst' in Fig. 12), the bubbles rebound. Then, after a ~300 μs prolonged expansion phase, collapse to generate the second burst.*

The goal of the project was to build a passive device which could continuously monitor these signals and interpret them in terms of the integrity of the ESWL targeting and the degree of stone fragmentation. The advances through the stages of the development of the device are as follows. For conciseness, the *in vitro* (§2.1(*a*)), CFD (§2.1(*b*)) and clinical (§2.1(*c*)) components will be described separately, although in fact the interaction between the two was a major feature of the project.

2.1(a) In vitro experimental work

a(i) A survey of the relevant *in vitro* and *in vivo* data was conducted and, by comparison with the Gilmore-Akulichev model for a spherical bubble, interpreted to estimate the likely initial radii of bubbles subjected to lithotripter pulses [7]. This key stage was vital, since the CFD work (see below) required knowledge of that initial bubble size. This provided the insight that the final stages of bubble oscillation were sufficiently low amplitude to allow their frequency to be related to bubble size (which would not have been appropriate during the earlier high-

amplitude stages of oscillation, prior to the majority of dissipative losses). Use of the Gilmore-Akulichev spherical bubble model was also more relevant at this stage than the jetting stages (see §2.2(*b*), below). Since pulses occur at intervals of several hundred milliseconds, the bubble size at the end of a preceding lithotripter exposure would provide the appropriate initial bubble size for most exposures, rather than the naturally-occurring *in vivo* ambient bubble population (which is unknown, and would only be relevant at the outset of treatment).

a(ii) A previously non-operational lithotripter was commissioned for use in laboratory *in vitro* tests.

a(iii) A series of staged hydrophone measurements *in vitro*, with and without a stone present, allowed characterisation (in terms of frequency, amplitude and timing) of the basic characteristics of the emissions upon which the sensor prototypes would be based [8].

a(iv) The results of *a(iii)* allowed further *in vitro* tests to compare hydrophone measurements with the signals from a prototype device built by the National Physical Laboratory to measure cavitation in industrial situations [8] (Fig. 4*a*). This collaboration benefited both organisations (the NPL system was a useful one to study, but would have been inappropriate for *in vivo* use).

a(v) The results of *a(iii)* and *a(iv)* allowed the collaborative design of a prototype device with its manufacturers, Precision Acoustics Ltd. (PAL). Subsequent *in vitro* and *in vivo* testing of this, and a second refined prototype, allowed development of the third, and final, prototype (Fig. 4) [9].

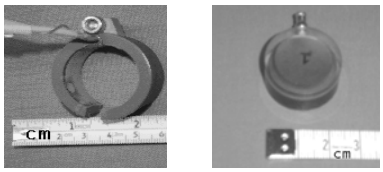

Fig. 4*. The NPL sensor (left) and the refined Precision Acoustics prototype (right).*

2.1(b) Simulation and modelling

b(i) A two-dimensional Free-Lagrange code for bubble collapse was investigated [10,11] and then adapted for three-dimensional axi-symmetric cases [12,13].

b(ii) Near field pressures were predicted for lithotripter-like cavitation events without solids present.

b(iii) Near field pressures were predicted for lithotripter-like cavitation events with plane solid half-spaces present (the solids having real material parameters, rather than simply being represented by rigid boundaries) [14].

b(iv) Near field pressures were predicted for lithotripter-like cavitation events with solids containing notches present [14].

b(v) Related work [15] predicted the stresses within an elastic-plastic solid half-space close to a cavitation bubble. In addition to mapping these (and their evolution in time), an index indicating approach to material failure and its evolution in the solid was plotted [14].

b(vi) An initial estimation of the associated far-field pressures was made using the Helmholtz-Kirchoff method. Although this assumes linear propagation of the emissions, and hence at this stage contained engineering approximations whose effects had not been quantified, nevertheless the agreement with clinical measurements was extremely good [20].

b(vii) The far-field calculations were extended to cover the acoustic emissions from populations of thousands of bubbles, distributed throughout the cigar-shaped focus of the lithotripter field [14].

b(viii) The initial approximation of *b(vi)* was improved by using the Ffowcs-Williams-Hawkings method [14].

b(ix) Recognising that the procedure of *b(viii)* cannot describe any nonlinearities in the propagation, the size of these were estimated using nonlinear propagation theory to examine propagation from the CFD near-field domain to the measurement point of the clinical sensor [14].

b(x) A nonlinear propagation theory was developed for transient acoustic waves in bubbly water such as might be found near the lithotripter focus [16,17,18].

b(xi) The work has been extended from single bubbles to predict at far field the emission from thousands of bubbles, distributed throughout the cigar-shaped focus of the lithotripter. This has produced new insights, particularly into how the duration of the bursts (**d1** and **d2** in Fig. 6) relate to the position of the sensor on the torso and the activity within the body.

2.1(c) Clinical work

c(i) In the empirical tests (whereby a surgeon is supplied with an audio-frequency representation of the device output and becomes accustomed to which signals typify good and bad outcomes of ESWL) the three clinicians scored 100% in correctly identifying the features which would pertain to a clinical evaluation of the success of the treatment.

c(ii) The *in vitro* tests of *a(iii)-a(v)*, particularly with the final prototype, enabled a range of characteristics to be identified for testing in the clinical environment, to determine the extent to which they indicate targeting and stone fragmentation [9,19]. These were compared with the predictions of CFD and the level of agreement was very encouraging (compare 'first burst; in Fig. 3 with Fig. 12; and see §2.2(*c*) for comparison of Figs. 8, 11 & 14) [20]. This enabled objective criteria to be drawn up, upon which the interpretive protocols on the final device are based.

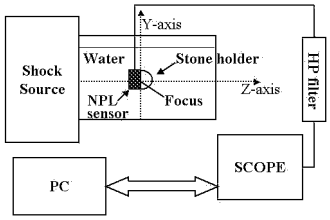

Fig. 5. *Experimental set-up for in vitro tests involving 'ping-pong' ball target holder (see §2.2(a)).*

2.2 Science and technology

2.2(a) In vitro experimental work

The *in vitro* tests were wide-ranging. An example is shown in Fig. 5. Stone phantoms are placed either at the focus of the lithotripter, or at known locations in relation to it. A variety of types were used, often placed within a ping-pong ball which was otherwise water-filled. A common method was to fill the ball with material containing roughly the same grain size, the tolerance being broader when sands and gravels were used (+/- 25%) than when grades of glass sphere were used (+/- 15%). The acoustic signals detected in the far field were parameterised in terms of the peak pressure amplitudes of the first and second bursts (as defined in Fig. 3), their respective durations, powers, spectral content and the interval between them (Figs. 6 and 7).

It is expected that the most reliable predictor of the degree of fragmentation will be based on a Principle Component (PC) or Multi-Variate (MV) analysis [23]. As the database increases, so too will the reliability of this approach. The dataset is currently being enhanced using follow-on funds, but the results to date are very promising (Fig. 8, lower plot). As an indicator of the potential of the approach, the upper plot of Fig. 8 illustrates what may be achieved with a single parameter, the peak pressure amplitude of the first burst. The peak amplitude **m1** of the first burst (see Fig. 6), normalised against the mass of the stone phantom for *in vitro* tests, is plotted again the grain size (Fig. 8), upper plot). There is a clear trend, the normalised amplitude decreasing as the grain size decreases (a trend which is also apparent when the amplitude plotted is **m1**, and not the ratio of **m1** to the phantom mass [9]). A simple understanding of this is that the stone fragments provide less acoustic return than a coherent stone, although the true picture involves the presence of liquid to nucleate cavitation and details of this have been

revealed by the CFD [14]. Hence in extrapolating from Fig. 8 to the *in vivo* case, one might replace the current abscissa with some time axis covering the duration of the treatment (as Fig. 14 eventually proved – see §2.2*c*,*d*).

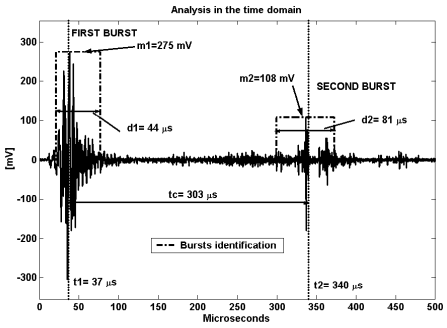

Fig. 6. *Example of the time domain analysis of an in vitro signal:* $\boldsymbol{m_1}$*=maximum amplitude of the first burst;* $\boldsymbol{d_1}$*=duration of the first burst;* $\boldsymbol{t_1}$*=central time of the first burst;* $\boldsymbol{t_c}$*=collapse time;* $\boldsymbol{m_2}$*=maximum amplitude of the second burst;* $\boldsymbol{d_2}$*=duration of the second burst;* $\boldsymbol{t_2}$*=central time of the second burst. The picture does not illustrate the kurtosis, which was used as a measure of the degree to which the bursts are 'peaked'.*

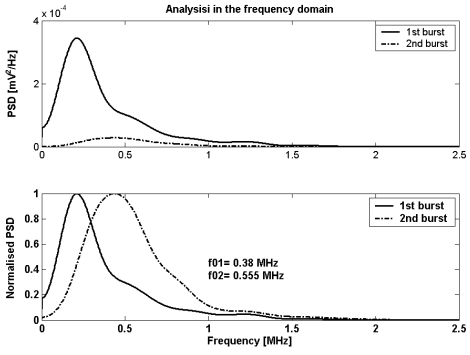

Fig. 7*. Example of the frequency domain analysis of an in vitro signal. The upper plot shows the power spectral density (PSD) of the first burst (solid line) and the second burst (dotted line). The former contains a greater proportion of lower frequency energy (<0.5 MHz) because in addition to cavitation emissions, it contains the reflected energy of the incident lithotripter pulse (which the second burst lacks). To illustrate this more clearly, in the lower plot the two PSDs from the upper plot are normalised of the two burst (upper box).*

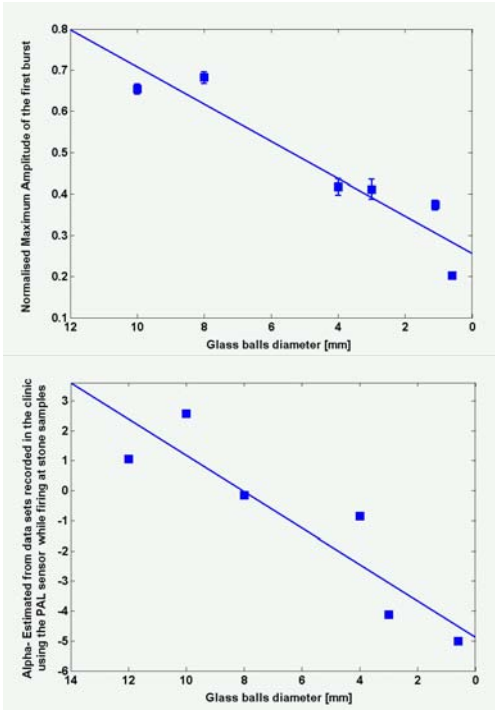

Fig. 8. *Glass spheres contained within the ping-pong ball are insonified in vitro by the lithotripter used in the clinical tests. Upper plot: the value of* ***m1*** *(see Fig. 6), normalised to the mass of glass present, as a function of glass sphere diameter. Lower plot: the mantissa is Alpha=(a1**$\boldsymbol{m1}$*+a2**$\boldsymbol{m2}$*+a3**$\boldsymbol{tc}$*) with a1, a2, a3 estimated using Principal Component Analysis.*

2.2(b). Computational Fluid Dynamics

For over a decade, the state-of-the-art method for computing the bubble response and the associated pressure emissions associated with lithotripsy has been the Gilmore-Akulichev (GA) model (see [4,5], Fig. 2). Whilst it has proved to be very useful, two of the inherent assumptions in the method are violated by the very nature of the stone fragmentation problem, making it imperative that a new approach be developed. Specifically, if the bubble is to fragment the stone through the production of a liquid jet, then there must be a stone present (violating the assumption in the GA model that the bubble exists in an infinite body of liquid); and the bubble must lose the sphericity which the GA model assumes it has at all times, in order to produce a jet. Of the available alternatives, the Boundary Integral Method [21] is inapplicable since it assumes that the liquid is irrotational and incompressible, making acoustic phenomenon (such as the propagation of a blast wave to far field) impossible; and in the Arbitrary Lagrangian Eulerian method [22], the mesh must cease to be Lagrangian prior to jet impact in order to avoid mesh tangling, leading to some loss of accuracy through numerical diffusion. The Free-Lagrange method suffers neither of these limitations, giving a fully compressible treatment on a mesh that remains Lagrangian at all stages of the cavitation process [14].

This should put perspective on the CFD achievements of this contract. Given the above comments on the previous studies, the first stage therefore provided a significant advance on the two approaches cited above [21,22], in that liquid compressibility was incorporated, and physically correct wave propagation in gas and liquid phases was obtained [14], for the jetting collapse of a single bubble (Fig. 9). This contract went much further, providing techniques for incorporating solids close to the bubble, and showing techniques by which those boundaries may incorporate cracks and notches (Fig. 10), by assigning real material properties to the solid and calculating the stresses within it (Fig. 10a), and also mapping the evolution of an index reflecting the likelihood of failure (Fig. 10b).

Fig. 11 shows the predicted '**m1**' pressure (as defined in Fig. 6) from a single cavitation bubble, which the clinical device would detect on the surface of the skin, in four possible scenarios (pure water (dotted line); bubble but no solid present (dashed line); solid but no bubble present (dot-dash line); both solid and bubble present (solid line)). The figure indicates that amplitudes measured at the sensor would commence at ~13 kPa when the stone is intact and the focusing is good, enabling cavitation to occur close to the stone (i.e. the scenario for Fig. 11, solid line). However as the treatment progresses, if it is successful and the stone remains in the focus but fragments, the received signal should decrease in amplitude (e.g. Fig. 11, dashed line). [This trend is supported by that of the *in vitro* tests (Fig. 8) if, as described at end of §2.2(a), the abscissa is replaced by a time axis.] Similarly, if the focus moves off-target, a sudden drop in received signal is expected. If the targeting remains good but the stone fails to fragment, no change should be seen in the received signal. The degree to which these hypotheses were borne out in the clinic will be described in the next section (§2.2(*c*)). First, note in Fig. 12 that the modelling capability of Fig. 11 has been extended from single bubbles to clouds of many thousands of bubbles, distributed through the lithotripter focus.

2.2(c) Clinical results

EPSRC rules restrict the extent of clinical trials, such that only a limited amount of clinical data could be collected with the final prototype. However further funding from the Medical Physics Dept. of Guys' and St Thomas' Health Trust has allowed more extensive clinical trials to proceed, and these are on-going. Both these and the EPSRC clinical tests were subject to full Ethics and Safety Approval procedures.

Having illustrated in the *in vitro* work (§2.2(*a*)) that **m1** has potential for indicating the integrity of targeting and degree of fragmentation (Fig. 8), and through CFD (§2.2(*b*) taking this further to predict the likely time-dependency of **m1** during a successful treatment (see underlined hypothesis, above), this section will discuss the measurements of **m1** in the clinic.

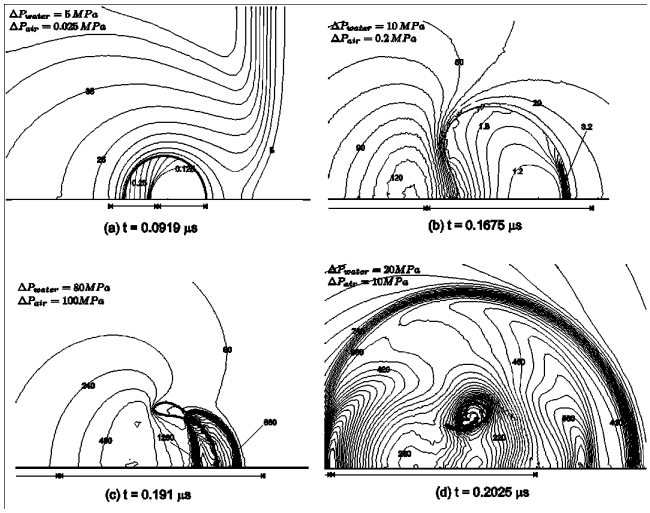

***Fig. 9 (left)**. An air of bubble of initial radius 40 microns in water is subjected in the free field to a lithotripter pulse (propagating from left to right). The response is predicted by the Vucalm hydrocode, the axis of rotational symmetry being the horizontal line at the base of each plot. The contour increments in pressure for both air and water are indicated on each plot, the value of selected contours being labelled in MPa (see [**Error! Bookmark not defined.**] for expanded version and movie). All elapsed times 't' are measured after the lithotripter pulse first meets the upstream bubble wall. (a) The lithotripter pulse has passed over the bubble, travelling further than the slower gas shock within the bubble. An expansion wave is reflected back off the bubble, travelling to the left and upwards in the picture. (b) The bubble involutes as it collapses, to form a liquid jet which will pass through the centre of the bubble. (c) The impact of the jet against the downstream bubble wall generates a blast wave, which propagates outwards in (d). Such liquid impacts and blast waves can generate erosion and biomechanical effects. The high temperatures and pressures attained within the gas can generate chemical effects and luminescence.*

***Fig. 10 (right).** The axis of rotational symmetry is the horizontal line at the base of each plot. (a) Stress (1 MPa contour intervals) in direction parallel to the axis of rotational for a bubble **initially with internal over-pressure** close to a plane surface (left frame) or close to a notched surface (right frame). Stress concentration resulting from the notch is apparent, indicating a likely effect of cracks in stones. The base of each frame is an axis of rotational symmetry. The vertical line in each frame divides the solid on the left from the liquid on the right. (b) For the same geometry as*

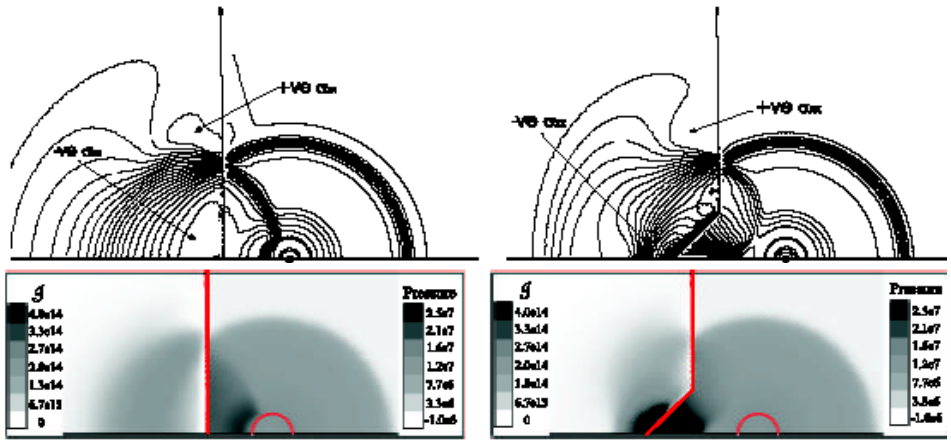

(a) this figure shows an index showing the likelihood of failure (see [14] for definition), where darker areas in the solid indicate a greater likelihood. The red line indicates the solid/liquid interface, and the red semicircle indicates the position of the bubble wall.

***Fig. 11 (right).** Predicted pressure time histories received at the sensor when it is placed 500 mm from the stone (typical clinical location on the surface of the skin). The time histories are for: a single cavitation bubble close to a stone (i.e. resembling the start of a well-targeted treatment - solid line); a single cavitation bubble with no stone present (i.e. resembling a poorly-targeted scenario – dashed line); a stone but no bubble present (dash-dot line); and neither bubble nor stone present (dotted line).*

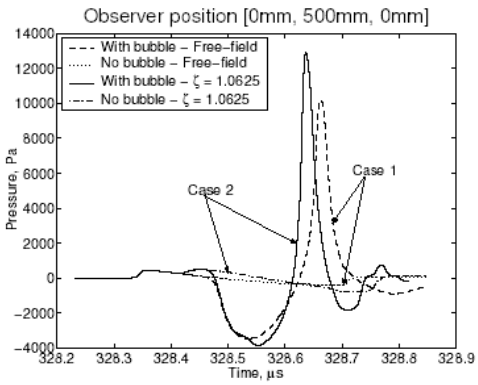

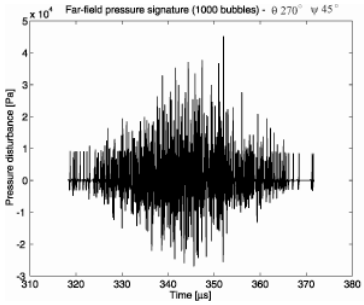

***Fig. 12 (above).** The predicted pressure time history of a 'first burst' (compare with signal measured in Fig. 3), 500 mm from focus centre, where 1000 bubbles are modelled as cavitating within the lithotripter focus. Here **m1** exceeds the ~13 kPa of Figs. 11 and 14 because a novel geometry was being simulated.*

***Fig. 13 (right).** Photograph of the apparatus in the clinic. At the extreme left of the image is half a PC screen, containing the stone X-ray of Fig. 1. Below is a detail of the sensor in place on the torso.*

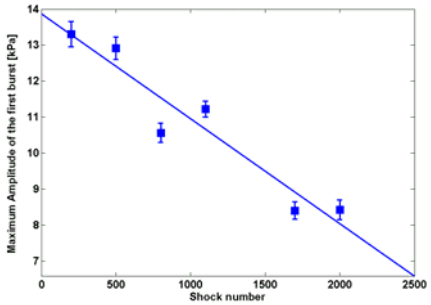

***Fig. 14 (above).** The peak amplitude **m1** of the first burst as time progresses for a successful treatment. Unsuccessful treatments showed a wide range of different behaviour* [23].

It must be remembered that **m1** represents just a single parameter of those illustrate in Fig. 6, and indeed even better predictors show promise through PC/MV Analysis [23] for which the follow-on support is providing clinical data. In this case, however, the correlation is not being made with a readily quantifiable parameter (the diameter of a glass sphere), but the rather imprecise terms in which the clinician expresses the success or otherwise of a given treatment. It is this very imprecision which justifies the need for the device, but it does make the PC/MV Analysis rather laborious.

Fig. 13 shows the device in the clinic. Fig. 14 shows the results for the value of **m1** during a successful treatment. Not only does the trend in the amplitude of the returned signal follow the trend expected from the *in vitro* tests (compare Fig. 14 with Fig. 8*a*). The absolute amplitudes of the received signal are consistent with those predicted by the CFD, starting at ~13 kPa and steadily decreasing (see the underlined hypotheses on page 3). The PC analysis has produced promising results, but clinical trial data is still being collected as part of the follow-on contract [23].

In addition to this objective analysis, three clinicians who operate the lithotripter in the normal course of their duties were played, in the audio regime, decimated 0-8 kHz representations of the 0-1 MHz signal detected by the PAL sensor. In randomised order, they heard 3 pre-recorded signals, pertaining to a successful treatment, an unsuccessful treatment, and a treatment which the clinicians had judged to be only slightly successful. The clinicans were not aware of these judgements prior to the test. Of the thousands of PAL signals detected during a treatment, only the first and last three were played (because of the limited time availability of clinicians for this trial). The tests were carried out within the usual protocols for subjective listening tests. All three clinicians scored 100% in interpreting the acoustic signal to guess the known outcome of the treatment on which a given recording was based.

2.2(d) Conclusions

Individually the experimental and simulation components have achieved a great deal. The CFD work in particular has provided software for axisymmetric Free Lagrange bubble collapses, which is utilised in new erosion grants (§6). Furthermore, the integration of the experimental and CFD components, to make and interpret a clinical device, has been highly successful. If the work were to be characterised by one 'eureka' moment, it would be when the absolute pressures measured in the clinic came out to be ~12 kPa, reducing as a successful treatment progressed (Fig. 14) as predicted by the CFD (Fig. 11). However it is recognised that this can only be the beginning of production of a final device for routine clinical use, and the work continues beyond the end of this EPSRC grant, in part as a result of further funding The Kirchoff-Helmholtz approach inherent in Figs. 11 & 12 is being improved upon (see above) and the effect of nonlinearities quantified. EPSRC rules limit the extent of the clinical trials they sponsor, and hence further trials are currently underway. The empirical feedback from three clinicians was 100% successful, and whilst this study was limited by the availability of surgeons, the results are extremely promising. The effectiveness of the PA/MV approaches is being refined as further clinical data on which to base the analysis is gathered. In summary, the device appears to perform extremely well when used both as an objective and a subjective measure of the efficacy of particular lithotripter treatment.

REFERENCES

1 **Leighton T G.** From sea to surgeries, from babbling brooks to baby scans: bubble acoustics at ISVR. *Proceedings of the Institute of Acoustics*, **26**, Part 1, 357-381, 2004, 357-381 (TYNDALL MEDAL PAPER)

2 **Leighton TG**. The acoustics of gas bubbles in liquids. *Anglo-French Physical Acoustics Group Meeting,* (Institute of Physics), 2001, p. 7 (**Keynote paper for Inaugural Meeting of this Group**)

3 **Leighton T G, Coleman AJ, Fedele F** & **White P R**, A passive acoustic system for evaluating the in vivo performance of extracorporeal shock wave lithotripsy. *UK Patent No. 0319863.7*

4 **Coleman A J, Choi M J, Saunders J E** & **Leighton T G**, Acoustic emission and sonoluminescence due to cavitation at the beam focus of an electrohydraulic shock wave lithotripter, *Ultrasound in Medicine and Biology*, **18**, 1992, 267-281

5 **Coleman A J, Whitlock M, Leighton T G** & **Saunders J E**, The spatial distribution of cavitation induced acoustic emission, sonoluminescence and cell lysis in the field of a shock wave lithotripter, *Phys. Med. Biol.*, **38**, 1993, 1545-60

6 **Leighton TG**. Characterization of measures of reference acoustic cavitation (COMORAC). *J. Acoust. Soc. Am.*, **108**(5), Part 2, 2000, 2516. (INVITED PAPER)

7 **Cunningham K B, Coleman A, Leighton T G** & **White P R**. Characterising in vivo acoustic cavitation during lithotripsy with time-frequency methods. *Acoustics Bulletin* **26**(5), 2001, 10-16

8 **Fedele F, Coleman AJ** & **Leighton TG**. Use of a cylindrical PVdF hydrophone in a study of cavitation adjacent to stone phantoms during extracorporeal shockwave lithotripsy. *Proc of the 9th Annual National Conference of the Institute of Physics and Engineering in Medicine*, (IPEM, Bath) p. 66, 2003

9 **Fedele F, Coleman AJ, Leighton TG, White PR** & **Hurrell AM**. A new diagnostic sensor for Extra-corporeal Shock-Wave Lithotripsy. *Acoustics Bulletin*, **29**, 2004, 34-39

10 **Ball GJ, Howell BP, Leighton TG** & **Schofield MJ,** Shock-induced collapse of cylindrical air cavity in water: Free-Lagrange simulation. *Shock Waves*, **10**, 2000, 265-76

11 **Ball GJ, Howell BP, Leighton TG** & **Schofield MJ**, Shock-induced collapse of a cylindrical air cavity in water: a Free-Lagrange simulation. *Proc. 22nd Int. Symposium on Shock Waves, London, July 1999, Paper 0060*, published April 2000, 1363-1368

12 **Jamaluddin AR, Ball GJ** & **Leighton TG**. Free-Lagrange simulations of shock/bubble interaction in shock wave lithotripsy. *The 24th International Symposium on Shock Waves, Beijing, China*, July 11 16, 2004 (in press)

13 **Jamaluddin AR, Ball GJ** & **Leighton TG.** Free-Lagrange simulations of shock/bubble interaction in shock wave lithotripsy. *Proc. 2nd Int. Conf. on Computational Fluid Dynamics, ICCFD, Sydney, Australia*, 15-19 July 2002, pp 541-546

14 **Jamaluddin AR, Turangan CK, Ball GJ** & **Leighton TG.** Free-Lagrange simulations of the jetting collapse of air bubbles with application to extracorporeal shock wave lithotripsy. *Proceedings of the Royal Society A* (in preparation)

15 **Turangan CK** & **Ball GJ.** A Free-Lagrange Simulation of Cavitation Bubble collase near a Rigid Boundary. The 23rd International Symposium on Shock Waves, Fort-Worth TX, USA, July 2001, pp793-799

16 **Leighton TG, Meers SD** & **White PR.** A nonlinear time-dependent inversion to obtain bubble populations from acoustic propagation characteristics. *Proceedings of the Royal Society* (in press; publ.Royal Society FirstCite Website May 2004)

17 **Leighton TG** & **Dumbrell HA**. New approaches to contrast agent modelling. *Proceedings of the First Conference in Advanced Metrology for Ultrasound in Medicine* (Journal of Physics Conference Series) (2004, accepted).

18 **Leighton TG** & **Dumbrell HA**. Modeling acoustic propagation through clouds of nonlinearly pulsating bubbles in *vivo*. *Ultrasound Med.Biol.* (2004, in preparation)
19 **Fedele F, Coleman AJ, Leighton TG, White PR** & **Hurrell AM.** A new sensor for detecting & characterising acoustic cavitation in vivo during ESWL. *Proceedings of the Institute of Acoustics*, **26**, Part 1, 2004, 422-432
20 **Leighton TG** 'From babbling brooks to baby scans, from seas to surgeries: The pressure fields produced by non-interacting spherical bubbles at low & medium amplitudes of pulsation', *International Journal of Modern Physics B* (in preparation) 2004
21 **Blake JR, Hooton MC, Robinson PB** & **Tong RP**. Collapsing cavities, toroidal bubbles & jet impact. *Phil. Trans. R. Soc. Lond. A* **355**, 1997, 537-550
22 **Ding Z** & **Graceswki SM**. The behaviour of a gas cavity impacted by a weak or strong shock wave. *J. Fluid Mech* **309**, 1996, 183-209
23 **Leighton TG, Fedele F, Coleman AJ, Jamaluddin AR, Ball GJ, White PR** & **Hurrell AM.** An experimental investigation into a passive sensor for continuous monitoring of targeting & stone fragmentation during ESWL. *Ultrasound Med. Biol. (in preparation)*